Spectral imbalance in the inertial range dynamics of decaying rotating turbulence

P. C. Valente[1] and V. Dallas[2]
[1]*LAETA/IDMEC, Instituto Superior Tecnico, Universidade de Lisboa, Av. Rovisco Pais, 1049-001 Lisboa, Portugal*
[2]*Department of Applied Mathematics, University of Leeds, Leeds LS2 9JT, United Kingdom*
(Received 17 October 2016; published 24 February 2017)

Direct numerical simulations of homogeneous decaying turbulence with background rotation show the existence of a systematic and significant imbalance between the non-linear energy cascade to small scales and its dissipation. By starting the decay from a statistically stationary and weakly rotating turbulent state, where the dissipation and the energy flux are approximately equal, the data show a growing imbalance between the two until a maximum is reached when the dissipation is about twice the energy flux. This dichotomy of behaviors during decay is reminiscent of the nonequilibrium and the equilibrium regions previously reported for nonrotating turbulence [Valente and Vassilicos, Phys. Rev. Lett. **108**, 214503 (2012)]. Note, however, that for decaying rotating turbulence the classical scaling of the dissipation rate $\epsilon \propto u'^3/L$ (where u' and L are the root mean square fluctuating velocity and the integral length scale, respectively) does not appear to hold during decay, which may be attributed to the effect of the background rotation on the energy cascade. On the other hand, the maximum energy flux holds the scaling $\Pi_{\max} \propto u'^3/L$ in the initial stage of the decay until the maximum imbalance is reached.

DOI: 10.1103/PhysRevE.95.023114

I. INTRODUCTION

Estimating the small-scale energy dissipation from large scale statistics for statistical stationary and nonstationary evolving flows is at the core of virtually all turbulence closures as it enables predictions of momentum transport (e.g., drag), mixing, particle dispersion and clustering, noise, etc. The emphasis is given to the empirical scaling of the energy dissipation rate $\varepsilon \propto u'^3/L$, using solely a characteristic turbulent velocity, such as the root mean square of the velocity fluctuations u', and an integral length scale L. This scaling is directly related to practical applications for modeling and goes back to the seminal works by Taylor [1] and Kolmogorov [2]. This inviscid scaling of the viscous dissipation rate of energy is supported by the widely accepted phenomenology that the small-scale dissipative turbulence-induced motions are fed by a continuous range of larger-scale motions (the energy cascade [3,4]), and are always sufficiently small scale to make molecular dissipation efficient (also known as the dissipation anomaly [3,5]).

The scale-by-scale energy budget for incompressible, externally forced, homogeneous flows in wave-number space can be written as [3,6]

$$\partial_t E(k,t) = T(k,t) - 2\nu k^2 E(k,t) + F(k,t), \qquad (1)$$

where $E(k,t)$ and $T(k,t)$ are, respectively, the spherically averaged energy spectrum and the net energy transfer term, $2\nu k^2 E(k)$ is the viscous dissipation spectrum, and $F(k,t)$ is the spectrum of energy input from the external forcing. Note that the energy budget is the same both for rotating and nonrotating flows [6]. Supposing that the external forcing is concentrated at small wave number k_f and integrating each term in Eq. (1) from $k > k_f$ to ∞ we get

$$\int_k^\infty \partial_t E(k',t)\,dk' = \Pi(k) - \int_k^\infty 2\nu k'^2 E(k',t)\,dk', \qquad (2)$$

where $\Pi(k,t) \equiv \int_k^\infty T(k',t)dk'$ is the nonlinear energy flux. It is generally accepted that for large Reynolds numbers and for k within the inertial range of scales $\int_k^\infty 2\nu k'^2 E(k',t)dk' \approx \varepsilon$ (i.e., the contribution of the large scales to the viscous dissipation is negligible) [7,8]. Here, the inertial range corresponds to scales sufficiently small not to have external energy input, i.e., $k > k_f$, but large enough for their contribution to the viscous dissipation to be negligible. Note that one cannot neglect $\int_k^\infty \partial_t E(k',t)\,dk'$ without introducing Kolmogorov's notion of local equilibrium [2] or restricting the scope to statistically steady turbulence where this term is identically zero and thus $\Pi(k) \approx \varepsilon$ for any k within the inertial range of scales, as long as the contribution to the viscous dissipation from $\int_0^k 2\nu k'^2 E(k',t)dk'$ is negligible, which is considered to be asymptotically exact for infinite Reynolds numbers. Kolmogorov's notion of local equilibrium assumes that small-scale turbulent motions are very fast paced and thus instantaneously adjust to dissipate whatever energy they are fed. The conceived near-instantaneous adjustment of the level of dissipation to the energy that the small scales receive from the large scales via the nonlinear flux [i.e., $\Pi(k) \approx \varepsilon$], is a landmark of the classical theory of turbulence and became popularized as Kolmogorov's 4/5th law due to its isotropic form [3,9,10]. The generalization that $\int_k^\infty \partial_t E(k',t)\,dk' \approx 0$ and therefore $\Pi(k) \approx \varepsilon$ for virtually all turbulent flows justifies its importance for turbulence modeling and its use as a building block in state-of-the-art closures.

Consequently, for decaying or generally nonstationary flows the spectral balance $\Pi(k) \approx \varepsilon$ [or $\Pi(k) = \varepsilon$ at infinitely large Reynolds numbers] is not exact and requires empirical testing to support its use in turbulence closures. Even for statistically steady flows at very large Reynolds numbers, the balance $\Pi(k) = \varepsilon$ is exact in a statistical sense where the quantities $\Pi(k)$ and ε are taken as averages in time and in the homogeneous directions and it is known not to hold in a local sense [11–13]. However, for nonstationary flows the balance $\Pi(k) = \varepsilon$ is yet to be observed—a fact that is usually attributed

either to the data being at insufficiently high Reynolds numbers (i.e., a low Reynolds number effect [7,14]) or, contrastingly, a consequence of the delay in cascading the energy down to the small scales (a lag which increases with the Reynolds number [11,15–18]).

A third, alternative, viewpoint is that, regardless of the Reynolds number and/or of energy cascade "delays," one cannot neglect the required rate of change of energy to induce or annihilate small scale motions $\int_k^\infty \partial_t E(k',t)\,dk'$ [19]. This is argued to be the case because even though the fraction of the total energy contained in the small scales K_η decreases with the Reynolds numbers, the associated time scale τ_η also becomes vanishingly small and it can be shown that $K_\eta/\tau_\eta \propto \varepsilon$ and is thus finite. This can be argued to be the root cause for the significant imbalance between $\Pi(k)$ and ε reported for nonstationary homogeneous turbulence and the manifestations of nonequilibrium dissipation behavior observed in recent experiments and simulations [8,19–23].

Many of the considerations above are also applicable for weakly rotating turbulent flows, i.e., flows where rotation has an important role on turbulence dynamics but it does not fully dominate the flow and lead to a quasi-2D turbulence regime [24–28]. For example, the empirical scaling $\varepsilon \propto u'^3/L$ is thought to apply to weakly rotating turbulence [28] with different variants to take into account the anisotropy of the flow [29,30]. In contrast, strongly rotating flows are weakly turbulent and exhibit marked differences such as laminarlike dissipation scaling [28] and thus the discussions pertaining to turbulence theory are of limited use. Furthermore, this weak rotation regime has, arguably, a closer connection to engineering applications and is also typical of many rotating turbulence laboratory experiments and numerical simulations [24,28,31–35].

In this paper, we investigate the existence of significant imbalances between $\Pi(k)$ and ε and nonequilibrium dissipation scalings in weakly rotating decaying flows. Therefore, we perform direct numerical simulations (DNSs) of decaying periodic box turbulence subject to different background rotation rates Ω and we create the conditions for nonequilibrium dissipation scalings by using a statistically steady and fully developed rotating turbulence field as an initial condition [19].

II. NUMERICAL METHODOLOGY

In this study, we consider the three-dimensional (3D) incompressible Navier-Stokes equations in a rotating frame of reference

$$\partial_t \boldsymbol{u} + \boldsymbol{\omega} \times \boldsymbol{u} + 2\boldsymbol{\Omega} \times \boldsymbol{u} = -\boldsymbol{\nabla} P + \nu \nabla^2 \boldsymbol{u}, \tag{3}$$

where $\boldsymbol{u}$ is the velocity field, $\boldsymbol{\omega} = \boldsymbol{\nabla} \times \boldsymbol{u}$ is the vorticity, $P = p/\rho + u^2/2$ is the total pressure per unit mass, ρ is the mass density, and ν is the kinematic viscosity. In a Cartesian domain, we choose the rotation axis to be in the z direction with $\boldsymbol{\Omega} = \Omega \boldsymbol{e}_z$, where Ω is the rotation frequency. In the ideal case of $\nu = 0$, Eq. (3) conserves the energy $E = \frac{1}{2}\langle |\boldsymbol{u}|^2 \rangle$ (where $|\cdot|$ stands for the L_2 norm) and the helicity $H = \langle \boldsymbol{u} \cdot \boldsymbol{\omega} \rangle$ with the angular brackets denoting a spatial average.

We numerically integrate Eq. (3) using the pseudospectral method in a periodic box of size 2π satisfying the incompressibility condition $\boldsymbol{\nabla} \cdot \boldsymbol{u} = 0$ and using a third-order Runge-Kutta scheme for the temporal advancement. The aliasing errors are removed with the 2/3 dealiasing rule and as a result the minimum and maximum wave numbers are $k_{\min} = 1$ and $k_{\max} = N/3$, respectively, where N is the number of grid points in each Cartesian coordinate. For more details on the numerical code, see Ref. [36].

The initial conditions for the decaying simulations are obtained by running the code with an additional nonhelical random forcing term (see [27,37]) until a statistically steady and fully developed turbulence state is reached. All simulations were integrated for more than 100 turnover times with the exception of the highest resolution runs (1024^3), which were integrated for roughly 80 turnover times. Then, the free turbulence decay was initiated by switching off the forcing.

The turbulent energy K, the energy dissipation rate ε, and the integral scale L are extracted from the spherical-shell averaged energy spectrum $E(k) \equiv \sum_{k \leqslant |\boldsymbol{k}| < k+1} |\widehat{\boldsymbol{u}}_{\boldsymbol{k}}|^2$, as

$$K \equiv \sum_k E(k), \tag{4}$$

$$\varepsilon \equiv 2\nu \sum_k k^2 E(k), \tag{5}$$

$$L \equiv 3\pi/(4K) \sum_k E(k)/k, \tag{6}$$

where $\widehat{\cdot}$ denotes the Fourier mode. The energy flux at wave number k is computed as

$$\Pi(k) \equiv -\sum_{k' \leqslant k} T(k') \quad \text{with} \tag{7}$$

$$T(k) \equiv \sum_{k \leqslant |\boldsymbol{k}| < k+1} \widehat{\boldsymbol{u}}^*(\boldsymbol{k}) \cdot \widehat{(\boldsymbol{u} \times \boldsymbol{\omega})}_{\boldsymbol{k}} \tag{8}$$

the nonlinear energy transfer term (* denotes the complex conjugate), from which we compute the maximum downscale energy flux as $\Pi_{\max} \equiv \max[\Pi(k)]$. We characterize the energy cascade flux by its maximum value $\Pi_{\max}$ since the functional form of $\Pi(k)$ in the inertial range follows $\Pi(k) \propto \Pi_{\max}[1 - \alpha(k\eta)^{4/3}]$ for statistically steady turbulence assuming an energy spectrum $E(k) \propto k^{-5/3}$, where α is a numerical constant and $\eta \equiv (\nu^3/\varepsilon)^{1/4}$ is the Kolmogorov microscale [19,38].

Two sets of dimensionless control parameters for the simulations are defined based on the forcing amplitude and large scale turbulence statistics and characterize the turbulence field used as the initial condition. The forcing Reynolds and Rossby numbers are given by $\mathrm{Re}_F = U/(k_{\min}\nu)$ and by $\mathrm{Ro}_F = U k_{\min}/(2\Omega)$, respectively, where $U = (f_0/k_{\min})^{1/2}$ and f_0 is the forcing amplitude. From these definitions Re_F^2 is essentially the forcing Grashof number and Ro_F the ratio of the rotation period $\tau_w \propto \Omega^{-1}$ to the turnover time at the forcing scale $\tau_f = (U k_{\min})^{-1}$. The turbulence Reynolds and Rossby numbers are given by $\mathrm{Re}_L = u'L/\nu$ and $\mathrm{Ro}_L = u'/2\Omega L$, respectively, where $u' \equiv \sqrt{2/3K}$ is the root mean square of the fluctuating velocity. For convenience we also define the Taylor microscale based Reynolds number $\mathrm{Re}_\lambda = u'\lambda/\nu$ where $\lambda \equiv \sqrt{15\nu u'^2/\varepsilon}$ is the Taylor microscale. Note that Re_F and Ro_F are control parameters for which we do not require knowledge of the solution to be evaluated whereas Re_L, Ro_L,

TABLE I. Numerical parameters of the DNS. Note that the values for the resulting turbulence Reynolds and the Rossby numbers are given for the steady state used as initial condition for the decay. Dataset no. 14 was obtained with the numerical code used in Ref. [19].

No.	Re_F	Ro_F	Re_L	Re_λ	Ro_L	Ω	ν	N
1	200	5.0	60	36	2.5	0.1	5.0×10^{-3}	128
2	200	0.5	250	115	0.2	1.0	5.0×10^{-3}	128
3	667	10.0	180	73	6.3	0.05	1.5×10^{-3}	256
4	667	5.0	175	72	3.0	0.1	1.5×10^{-3}	256
5	667	1.0	220	80	0.6	0.5	1.5×10^{-3}	256
6	667	0.5	940	287	0.2	1.0	1.5×10^{-3}	256
7	2000	∞	500	130	∞	0.0	5.0×10^{-3}	512
8	2000	5.0	500	130	3.3	0.1	5.0×10^{-3}	512
9	2000	var	500	130	3.3	var	5.0×10^{-3}	512
10	2000	1.0	615	144	0.6	0.5	5.0×10^{-3}	512
11	2000	var	615	144	0.6	var	5.0×10^{-3}	512
12	2000	0.5	2410	414	0.2	1.0	5.0×10^{-3}	512
13	4545	5.0	1150	200	3.0	0.1	2.2×10^{-4}	1024
14		∞	924	173	∞	0.0	1.5×10^{-3}	1024

and Re_λ are observables and cannot be determined *a priori*. The summary of the control parameters of our DNS and the resulting turbulence Reynolds and Rossby numbers for the initial condition are listed in Table I.

According to Ref. [34], it is common practice in turbulence laboratory experiments to force briefly at Rossby numbers $\mathrm{Ro}_L > 1$, and then let Ro_L drift down to $\mathrm{Ro}_L \sim 1$ as the energy of the turbulence decays. Trying to perform numerical simulations that would be useful to laboratory experiments, we followed this approach to perform our DNS. As we shall see, this approach is rather different than the simulations which often have imposed $\mathrm{Ro} \ll 1$ as an initial condition.

To avoid biasing our analyses with data that may have non-negligible confinement effects due to the periodic box size we only consider data points where the integral length scale is smaller than 1/4 of the box size ($2\pi/L \gtrsim 4$; [39]), except for the strongly rotating cases (datasets no. 2, no. 6, and no. 12) where we alleviate this constraint to $2\pi/L \gtrsim 2.9$ (see Fig. 1). Nevertheless, we include the remaining data in the figures, but distinguish them using black marks and thin dashed lines.

III. RESULTS

The presented data complement the numerical and experimental data available in the literature in two fundamental aspects. First, we use forced statically steady state turbulence with the desired Rossby number as an initial condition rather than a randomized velocity field. This approach allows us to reproduce the conditions for nonequilibrium turbulence dissipation [19] and assess whether it also occurs in weakly rotating turbulence. It also guarantees that the turbulence is fully developed—in the sense of a fully developed energy cascade—from the very start of the decay in contrast to the standard approach where the first couple of eddy turnover times of the decay are biased by the development of the nonlinear interactions. This allows us to consider the data from the very start of the decay, where the nonequilibrium dissipation behavior is manifested, but comes at the price of

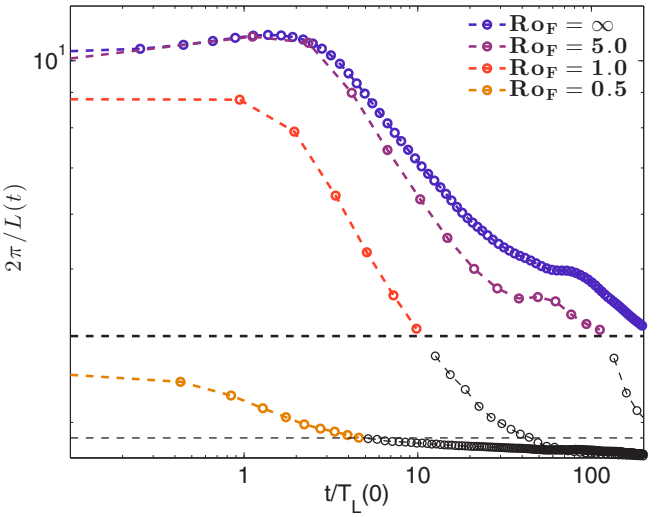

FIG. 1. Development of the ratio of the box size to the integral length scale, $2\pi/L$, throughout the decay for various control Rossby numbers Ro_F at $\mathrm{Re}_F = 2000$. The abscissas are normalized by the initial eddy turnover time. The data corresponding to $2\pi/L < 4$ (or $2\pi/L < 2.9$ for the strong rotation case, $\mathrm{Ro}_F = 0.5$) are denoted using black thin marks and dashed lines.

requiring a converged forced run for every decay simulation. Second, in addition to simulations with a constant rotation rate and thus decreasing Rossby number during decay (i.e., an increasing influence of the background rotation) we also perform decaying simulations with a constant Rossby number by varying the rotation rate. This, in turn, allows us to study the decay of turbulence subjected to rotation within the same rotating turbulence regime, i.e., maintaining the same ratio of the rotation period $\tau_w \propto \Omega^{-1}$ to the eddy turnover time $T_L = L/u'$ throughout the decay, and report differences to the standard approach of fixing Ω and thus straddling multiple rotating turbulence regimes during the decay (since T_L can increase by multiple orders of magnitude).

A. Temporal evolution

We start by presenting the temporal evolution of the turbulence statistics that will be used to show that in rotating turbulence there is also evidence of nonequilibrium dissipation scalings and of the imbalance $\Pi(k) \neq \varepsilon$ throughout the decay. The statistics of interest are the time series of the integral scale L (Fig. 1), the kinetic energy K (Fig. 3), the dissipation rate ε, and the maximum energy flux Π_{max} (Fig. 4) for a range of the control parameter Ro_F. As noted in Sec. II, box turbulence simulations can be hindered by confinement effects if the integral scale is not sufficiently smaller than the box size. The situation worsens for decaying box-turbulence simulations since the integral scale generally grows throughout the decay and thus the effects of confinement are progressively larger. We chose $2\pi/L \approx 4$ [39] as our cutoff beyond which the confinement effects may no longer be negligible (Fig. 1). For rotating turbulence, the integral scale tends to increase and grow faster during decay for smaller Rossby numbers (i.e., larger Ω), arguably due to the effect of the background rotation on the energy cascade [26,40,41], and therefore

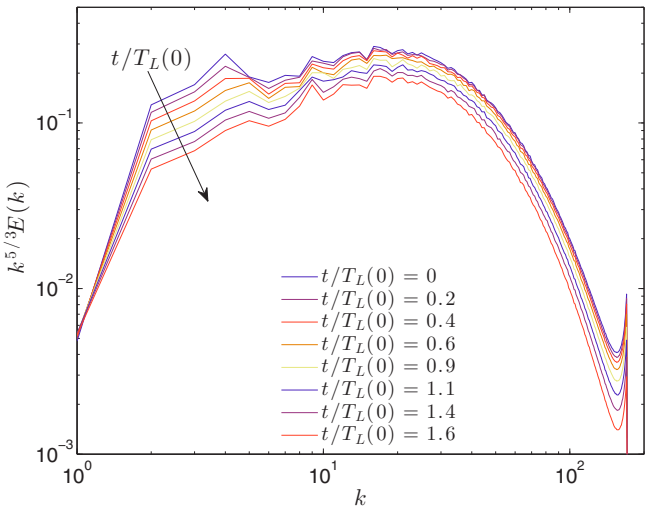

FIG. 2. Energy spectrum compensated by $k^{5/3}$ for the initial instants of the turbulence decay for $\mathrm{Ro}_F = \infty$ and $\mathrm{Re}_F = 2000$.

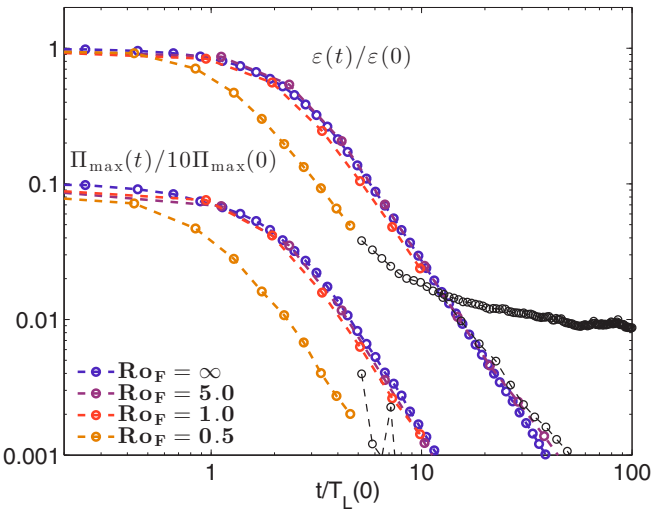

FIG. 4. Decay of the turbulent energy dissipation ε and the energy cascade flux Π for different control Rossby numbers Ro_F for $\mathrm{Re}_F = 2000$.

the confinement tends to deteriorate (Fig. 1). Note that at the start of the decay the integral scale decreases ($2\pi/L$ increases) for the first one or two turnover times before growing throughout the remaining decay. We observed this behavior for most of our simulations, except the strongly rotating cases. This behavior requires some discussion. Given that $L \equiv 3\pi/(4K)\sum_k E(k)/k$, the low wave-number part of the spectrum has a large influence on the numerical value of L and thus a decrease in L during a decrease in K implies that the smaller wave numbers are losing energy faster than the larger wave numbers (cf. Fig. 2). A plausible explanation is the adjustment of the low wave-number part of the spectrum to the cessation of external forcing—noticeable up to $t/T_L(0) \lesssim 0.4$ in Fig. 2.

In turn the energy decreases monotonically throughout the decay at a rate which depends on the initial Rossby number (Fig. 3), which is consistent with the numerical and experimental data in the literature [40–42]. Given that in freely decaying homogeneous turbulence $dK/dt = -\varepsilon$, this is a direct consequence of the faster decrease in the energy dissipation rate ε, which is a consequence of (or the cause for) the dampening of the nonlinear energy flux $\Pi(k)$ (Fig. 4). The energy flux spectra for various instances throughout the decay are shown in Fig. 5 for a dataset with moderately strong background rotation ($\mathrm{Ro}_F = 1.0$ and Ro_L decreases from 0.5 at the start of the decay to 0.1 when $2\pi/L < 4$; this dataset is included in Figs. 1, 3, and 4). It can be noted that the maximum value of the normalized flux spectrum $\Pi(k)/\varepsilon$ decreases as time progresses and that no upscale energy flux at low wave numbers occurs even at later times where the Rossby number is moderately low, $\mathrm{Ro}_L \approx 0.1$. Figure 5 also illustrates what

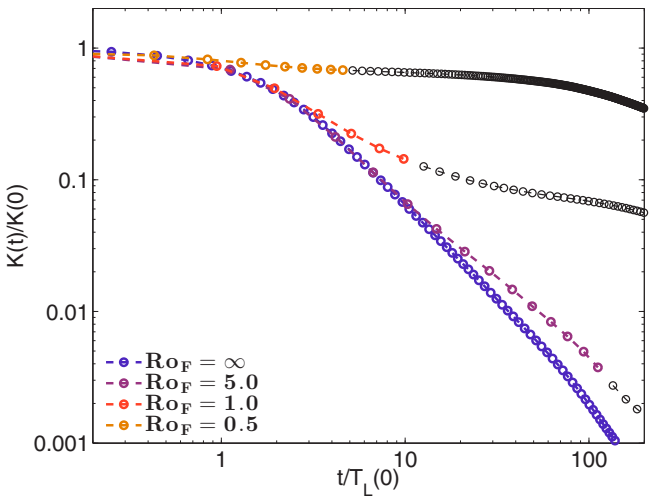

FIG. 3. Decay of energy over time (normalized by the initial eddy turnover time) for various control Rossby numbers Ro_F at $\mathrm{Re}_F = 2000$.

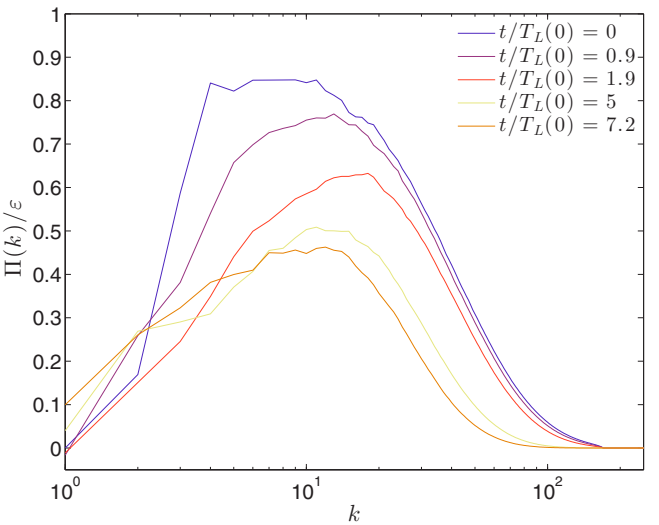

FIG. 5. Energy cascade flux spectrum $\Pi(k)$ for various snapshots throughout the decay for dataset no. 10 ($\mathrm{Re}_F = 2000$, $\mathrm{Ro}_F = 1.0$).

we mean by weakly rotating turbulence—turbulence where the background rotation has a significant effect on the energy cascade but not strong enough to induce an upscale energy flux and/or a quasi-2D flow.

B. Decaying nonrotating turbulence

Having turbulence modeling in mind, in the following discussion we chose to consider the dimensionless dissipation and energy flux parameters and how they may scale with large scale variables,

$$C_\varepsilon \equiv \varepsilon L/u'^3 \quad \text{and} \quad C_\Pi \equiv \Pi_{\max} L/u'^3, \tag{9}$$

respectively, without attempting to infer whether statistics decomposed along axes parallel and perpendicular to the axis of the rotation could improve the scalings (see, e.g., Ref. [43]).

Prior to discussing our results concerning the scaling behavior of these quantities in rotating turbulence, it is useful to review the recent developments for nonrotating turbulence to have it as a benchmark. In laboratory experiments of grid-generated decaying nonrotating turbulence it is widely accepted that far from the grid $\varepsilon \propto u'^3/L$ or $C_\varepsilon \approx$ const as long as the Reynolds number of the decaying turbulence remains moderately large, typically at least above $\mathrm{Re}_\lambda \approx 100$. Although until recently the scaling of the cascade flux had not been measured and the Reynolds number of the DNS data were insufficiently large, it was believed that in that same region $C_\Pi \approx C_\varepsilon \approx$ const. Recently, however, three interesting findings have been reported for both laboratory experiments and numerical simulations. First, it was found that upstream or after the steady-state region (i.e., $C_\varepsilon \approx C_\Pi$), there is a region where $C_\varepsilon \propto Re_0/Re_L \neq$ const, denoted as a nonequilibrium dissipation region [8,19,22] (where Re_0 is a global Reynolds number of the flow such as our control Reynolds number based on the forcing Re_F or a mesh Reynolds number for grid turbulence experiments). Second, it was found that in the further downstream region or later in time where $C_\varepsilon \approx$ const, the dissipation was roughly twice the nonlinear flux $\Pi_{\max}$ (i.e., $C_\varepsilon \approx 2C_\Pi$). Finally, it was found that C_Π exhibits much smaller variations and can be considered to a first approximation to being constant throughout the decay, contrary to what is observed for C_ε.

In Fig. 6 we present data for C_Π and C_ε from two DNSs of decaying nonrotating turbulence which are consistent with the above mentioned findings.

The steady state corresponds to the initial point where $\mathrm{Re}_L/\mathrm{Re}_L(0) = 1$ and $C_\Pi \approx C_\varepsilon$. As the turbulence decays, the Reynolds number decreases and the data show that C_ε increases from its steady state value around 0.5 until reaching a plateau starting around $\mathrm{Re}_L/\mathrm{Re}_L(0) \approx 0.5$ where it takes a

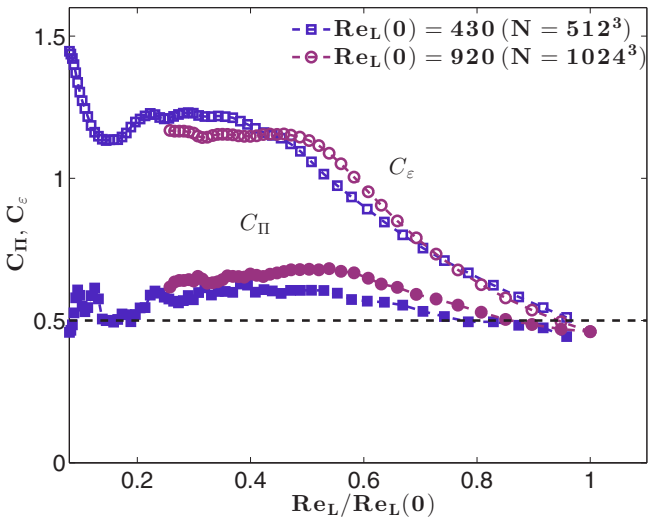

FIG. 6. Normalized turbulent energy dissipation C_ε and nonlinear energy cascade flux C_Π vs the turbulent Reynolds number Re_L for nonrotating decaying simulations starting from a statistically steady forced state.

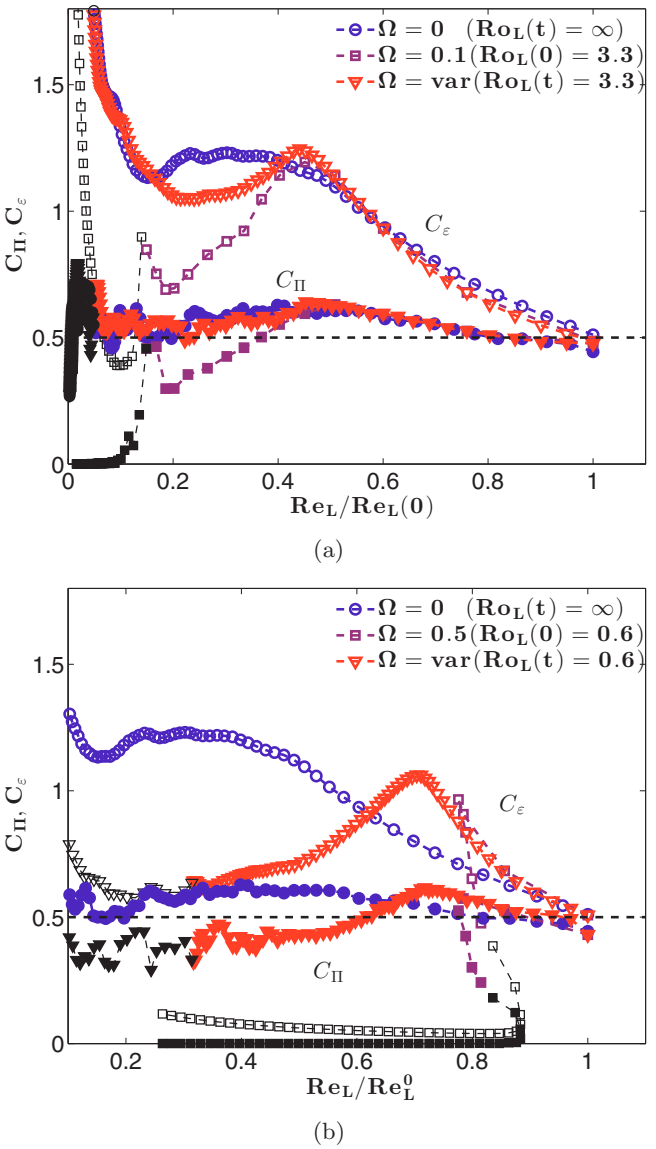

FIG. 7. Normalized turbulent energy dissipation C_ε and nonlinear energy cascade flux C_Π vs the turbulent Reynolds number Re_L for rotating and nonrotating decaying simulations starting from a statistically steady forced state. For the rotating cases we compare both constant rotation rate Ω (and varying Ro_L) and constant turbulent Rossby number Ro_L (achieved by varying Ω) simulations.

numerical value of order 1. This is the denoted nonequilibrium dissipation region exhibiting a clear departure from $C_\varepsilon \approx$ const, contrasting with the behavior C_Π which exhibits a lesser variation. As the turbulence continues to decay the Reynolds number will eventually decrease to a point where low Reynolds number effects will be non-negligible and C_ε will depart from the plateau with the numerical value of order 1, whereas C_Π remains approximately constant (see, e.g., Ref. [44] for a review on the low Reynolds number behavior of C_ε and data supporting $C_\Pi \approx$ const for low Reynolds numbers).

Note that the data presented in Fig. 6 were obtained with two distinct numerical codes. The lower Reynolds number data simulated with $N = 512^3$ collocation points were obtained with the numerical code used for the remaining rotating turbulence simulations, whereas the $N = 1024^3$ data were obtained with the numerical code used in Ref. [19]. Both numerical codes employ a pseudospectral method, but the forcing strategies for the steady state simulations serving as initial conditions for the decay are quite different. For more details please refer to Refs. [19,27].

It is thus reassuring to note that although there are quantitative differences, the qualitative behavior of C_Π and C_ε is quite similar.

C. Decaying rotating turbulence

Turning now to the decaying rotating turbulence, it is clear that the same qualitative departure between C_Π and C_ε occurs from the start of the decay for both cases of weak ($\mathrm{Ro}_L \approx 3.3$) and stronger rotation ($\mathrm{Ro}_L \approx 0.6$) and for both fixed and varying rotation rates (cf. Figs. 7 and 9).

However, rather than reaching a plateau, C_ε reaches a maximum value and decreases afterwards [see Figs. 7(a) and 7(b)]. Interestingly, this appears to be directly associated with the behavior of C_Π and how the nonlinear interactions are affected by the background rotation. For the runs with fixed background rotation rate, and therefore decreasing Ro_L as the turbulence decays, the associated dampening of the energy cascade leads to a diminishing value of C_Π which occurs progressively for the run with weaker background rotation [Fig. 7(a)] and very abruptly for the run with higher background rotation [Fig. 7(b)]. For the runs with fixed Ro_L throughout the decay (i.e., varying Ω), it is clear that the effect of the background rotation on the cascade leads to a reduced variation in the numerical value of C_Π throughout the decay. For the weaker rotation ($\mathrm{Ro}_L \approx 3.3$) the behavior of C_Π is almost identical to the nonrotating case [Fig. 7(a)], whereas for the stronger rotation ($\mathrm{Ro}_L \approx 0.6$), the normalized energy flux reaches a plateau around $C_\Pi \approx 0.4$ [Fig. 7(b)]. Interestingly, it appears that the behavior of C_ε beyond the initial increase appears to be dictated by the behavior of C_Π

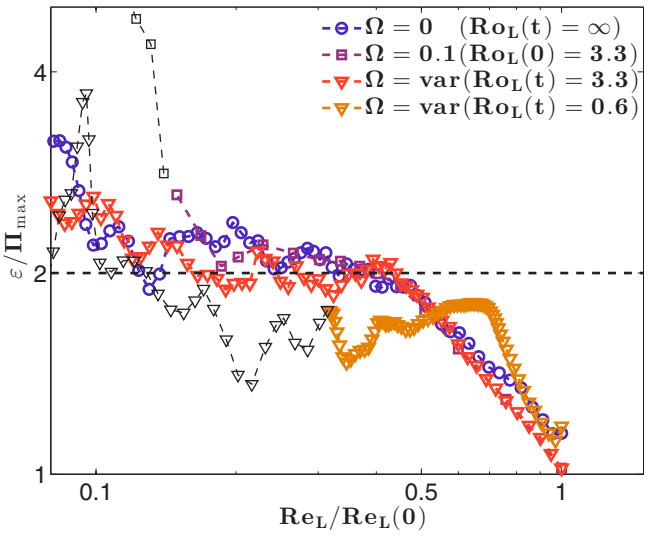

FIG. 8. Ratio between the turbulent energy dissipation ε and the maximum nonlinear energy cascade flux $\Pi_{\max}$ vs the turbulent Reynolds number $\mathrm{Re}_L/\mathrm{Re}_L(0)$ for rotating and nonrotating decaying simulations starting from a statistically steady forced state.

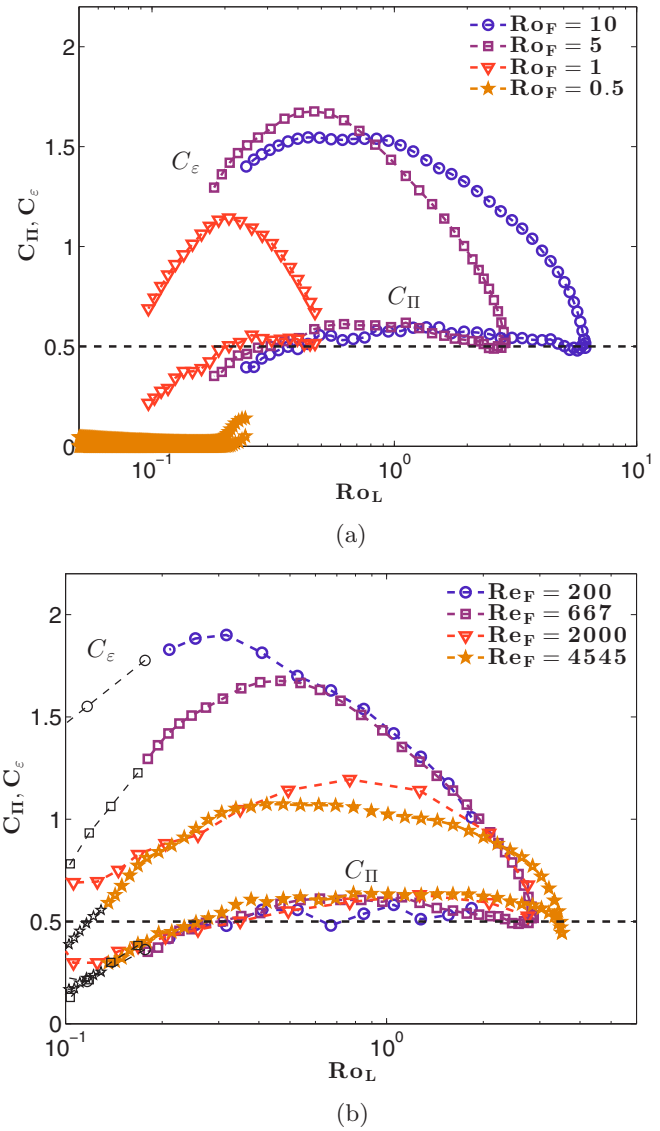

FIG. 9. Normalized turbulent energy dissipation C_ε and nonlinear energy cascade flux C_Π vs the turbulent Rossby number Ro_L for the rotating decaying simulations starting from a statistically steady forced state for (a) various control Rossby numbers Ro_F at a fixed $\mathrm{Re}_F = 667$ and (b) various control Reynolds numbers Re_F at a fixed $\mathrm{Ro}_F = 5.0$.

and the two seem to be proportional. Indeed, by plotting the ratio between ε and $\Pi_{\max}$ it can be seen that there is a period where $\varepsilon/\Pi_{\max} \approx$ const (with a constant around 2 or slightly lower for the stronger rotation case, which may nevertheless be due to confinement effects) after a transition region from the initial steady state where $\varepsilon \approx \Pi_{\max}$, similar to what is observed for nonrotating turbulence (cf. Fig. 8). As noted for nonrotating turbulence, as the turbulence continues to decay, the small Reynolds number effects become non-negligible and there is a monotonous increase in the ratio $\varepsilon/\Pi_{\max}$.

In Fig. 9, we show the behavior of C_Π and C_ε against the turbulent Rossby number Ro_L for various control Ro_F when $\mathrm{Re}_F = 667$ [Fig. 9(a)] and for various control Re_F when $\mathrm{Ro}_F = 5.0$ [Fig. 9(b)]. Interestingly, it appears that C_Π is roughly constant with a numerical value around 0.5 for $\mathrm{Ro}_L \gtrsim 0.3$ and decreases for smaller Ro_L. Note that C_Π is almost independent of the initial Rossby and Reynolds numbers as long as the initial Rossby number is sufficiently large to allow a fully turbulent flow for a given Reynolds number [28]. In turn, the behavior of C_ε for the various initial Rossby numbers is also qualitatively similar to that discussed above, i.e., presenting the initial ascending departure from $C_\varepsilon \approx C_\Pi$ followed by a descent which can be attributed to the effect of the background rotation on the energy cascade that is depicted as a decrease in C_Π.

Last, the behavior of C_ε for increasingly larger Re_F is such that the maximum value reached decreases [cf. Fig. 9(b)]. For even larger Reynolds numbers, it may be the case that the behavior of C_ε becomes Reynolds number independent with a functional form close to that indicated by our largest Reynolds number dataset in Fig. 9(b), but one cannot preclude the hypothesis that the departure of C_ε from C_Π will further decrease and eventually $C_\varepsilon \approx C_\Pi$, indicating that this behavior is a finite Reynolds number effect which vanishes at very large Re.

IV. CONCLUSIONS

Decaying turbulence subjected to background rotation exhibits similar imbalances between the energy flux $\Pi_{\max}$ and the energy dissipation rate ε as recently reported for laboratory and numerical experiments of freely decaying nonrotating turbulence [8,19]. In close resemblance to nonrotating turbulence, the ratio $\varepsilon/\Pi_{\max}$ increases from unity at the start of the decay, if the initial condition is statistically steady turbulence at sufficiently large Reynolds number, up to a value around 2 where it exhibits a plateau which ceases when the turbulence has decayed to a point where low Reynolds number effects become predominant.

At the initial stage of the decay the dimensionless parameter C_Π is approximately constant (i.e., $\Pi_{\max} \propto u'^3/L$), while C_ε increases up to a maximum value. In contrast to nonrotating turbulence, we find that C_ε does not exhibit a region where $C_\varepsilon \approx$ const (i.e., ε does not scale as u'^3/L). This appears to be related to the fact that C_Π tends to decrease after C_ε reaches a maximum value as the Rossby number and the Reynolds number decrease. The decrease in C_Π is commonly attributed to the dampening of the nonlinear energy cascade caused by the background rotation. We demonstrate this by introducing simulations with fixed turbulent Rossby number. In this case, it is possible to maintain a consistent effect of the rotation throughout the decay, which reduces the variation in C_Π and consequently the variation in C_ϵ.

Our data indicate that C_ε may not tend towards C_Π as the Reynolds number increases, but we are not able to address how this imbalance will behave at larger Reynolds numbers. However, for nonrotating flows the reader is referred to the discussion in Ref. [19] and the data compilation in Refs. [7,14] where the imbalance between ε and $\Pi_{\max}$ is suggested to persist up to at least $\mathrm{Re}_\lambda \sim \mathcal{O}(10^5)$, which implies that for the overwhelming majority of engineering applications one cannot neglect this behavior.

The fact that C_Π remains constant while C_ε exhibits significant variations during decay for the Reynolds and Rossby numbers that we considered implies that a turbulence model, in the spirit of the K-ε model, with an evolution equation for the energy flux instead of the energy dissipation rate would be more robust for the simulation of nonstationary flows ubiquitous in engineering applications. Nevertheless, in order to have a more complete picture, dedicated experiments are required to assess the imbalance $\Pi_{\max} \neq \varepsilon$ at much larger Reynolds numbers for both rotating and nonrotating turbulent flows that are statistically nonstationary. Until recently these investigations were limited to laboratory experiments but the computational capabilities to perform high Reynolds number numerical experiments are now becoming available.

ACKNOWLEDGMENTS

V.D. acknowledges support from the Royal Society and the British Academy of Sciences (Newton International Fellowship No. NF140631). The computations were performed on ARC1 and ARC2, part of the High Performance Computing facilities at the University of Leeds, UK. P.V. acknowledges support from COMPETE, FEDER, and Fundação para a Ciência e a Tecnologia (Grant No. PTDC/EME-MFE/113589/2009) on an early stage of the work and would like to thank Professor C. B. da Silva for making possible the nonrotating turbulence simulation with $N = 1024^3$ collocation points.

[1] G. I. Taylor, Proc. R. Soc. London, Ser. A **151**, 421 (1935); **151**, 444 (1935); **151**, 455 (1935).

[2] A. N. Kolmogorov, Dokl. Akad. Nauk. SSSR **30**, 301 (1941a); **31**, 538 (1941b); **32**, 16 (1941c); Izv. Akad. Nauk. SSSR Ser. Fiz. **6**, 56 (1942).

[3] U. Frisch, *Turbulence: The Legacy of A. N. Kolmogorov* (Cambridge University Press, Cambridge, England, 1995).

[4] M. Wan, Z. Xiao, C. Meneveau, G. L. Eyink, and S. Chen, Phys. Fluids **22**, 061702 (2010).

[5] G. L. Eyink, Nonlinearity **16**, 137 (2003).

[6] C. C. Lin, in *First Symposium of Applied Mathematics* (AMS, Providence, RI, 1947).

[7] J. Tchoufag, P. Sagaut, and C. Cambon, Phys. Fluids **24**, 015107 (2012).

[8] P. C. Valente and J. C. Vassilicos, Phys. Fluids **27**, 045103 (2015).
[9] S. B. Pope, *Turbulent Flows* (Cambridge University Press, Cambridge, England, 2000).
[10] C. Meneveau and J. Katz, Annu. Rev. Fluid Mech. **32**, 1 (2000).
[11] R. Kraichnan, J. Fluid Mech. **62**, 305 (1974).
[12] V. Borue and S. A. Orszag, J. Fluid Mech. **366**, 1 (1998).
[13] B. R. Pearson, T. A. Yousef, N. E. L. Haugen, A. Brandenburg, and P.-Å. Krogstad, Phys. Rev. E **70**, 056301 (2004).
[14] R. A. Antonia and P. Burattini, J. Fluid Mech. **550**, 175 (2006).
[15] J. L. Lumley, Phys. Fluids **4**, 203 (1992).
[16] A. Yoshizawa, Phys. Rev. E **49**, 4065 (1994).
[17] R. Rubinstein, T. T. Clark, D. Livescu, and L.-S. Luo, J. Turbul. **5**, 011 (2004).
[18] W. J. T. Bos, L. Shao, and J.-P. Bertoglio, Phys. Fluids **19**, 045101 (2007).
[19] P. C. Valente, R. Onishi, and C. B. da Silva, Phys. Rev. E **90**, 023003 (2014).
[20] K. Nagata, H. Suzuki, H. Sakai, Y. Hayase, and T. Kubo, Int. Rev. Phys. **5**, 400 (2008).
[21] P. Geipel, K. H. Henry Goh, and R. P. Lindstedt, Flow, Turbul. Combust. **85**, 397 (2010).
[22] P. C. Valente and J. C. Vassilicos, Phys. Rev. Lett. **108**, 214503 (2012).
[23] K. Nagata, Y. Sakai, T. Inaba, H. Suzuki, O. Terashima, and H. Suzuki, Phys. Fluids **25**, 065102 (2013).
[24] L. Bourouiba and P. Bartelo, J. Fluid Mech. **587**, 139 (2007).
[25] T. Teitelbaum and P. D. Mininni, Phys. Rev. Lett. **103**, 014501 (2009).
[26] A. Delache, C. Cambon, and F. Godeferd, Phys. Fluids **26**, 025104 (2014).
[27] V. Dallas and S. M. Tobias, J. Fluid Mech. **798**, 682 (2016).
[28] A. Alexakis, J. Fluid Mech. **769**, 46 (2015).
[29] K. D. Squires, J. R. Chasnov, N. N. Mansour, and C. Cambon, in *74th Fluid Dynamics Symposium on Application of Direct and Large Eddy Simulation to Transition and Turbulence, Chania, Greece* (1994).
[30] Y. B. Baqui and P. A. Davidson, Phys. Fluids **27**, 025107 (2015).
[31] L. Jacquin, O. Leuchter, C. Cambon, and J. Mathieu, J. Fluid Mech. **220**, 1 (1990).
[32] C. Morize, F. Moisy, and M. Rabaud, Phys. Fluids **17**, 095105 (2005).
[33] J. E. Ruppert-Felsot, O. Praud, E. Sharon, and H. L. Swinney, Phys. Rev. E **72**, 016311 (2005).
[34] P. A. Davidson, Y. Kaneda, and K. R. Sreenivasan, *Ten Chapters in Turbulence* (Cambridge University Press, Cambridge, England, 2012).
[35] F. S. Godeferd and F. Moisy, Appl. Mech. Rev. **67**, 030802 (2015).
[36] D. O. Gómez, P. D. Mininni, and P. Dmitruk, Phys. Scr. **T116**, 123 (2005).
[37] V. Dallas, S. Fauve, and A. Alexakis, Phys. Rev. Lett. **115**, 204501 (2015).
[38] T. Ishihara, T. Gotoh, and Y. Kaneda, Annu. Rev. Fluid Mech. **41**, 165 (2009).
[39] S. de Bruyn Kops and J. Riley, Phys. Fluids **10**, 2125 (1999).
[40] C. Morize and F. Moisy, Phys. Fluids **18**, 065107 (2006).
[41] T. Teitelbaum and P. D. Mininni, Phys. Fluids **23**, 065105 (2011).
[42] P. J. Staplehurst, P. A. Davidson, and S. B. Dalziel, J. Fluid Mech. **598**, 81 (2008).
[43] P. D. Mininni, A. Alexakis, and A. Pouquet, Phys. Fluids **21**, 015108 (2009).
[44] W. D. McComb, A. Berera, M. Salewski, and S. Yoffe, Phys. Fluids **22**, 061704 (2010).